BBA 75815

# HINDRANCE OF SOLUTE DIFFUSION WITHIN MEMBRANES AS MEASURED WITH MICROPOROUS MEMBRANES OF KNOWN PORE GEOMETRY

ROBERT E. BECK* AND JEROME S. SCHULTZ**

*Department of Chemical Engineering, University of Michigan, Ann Arbor, Mich. (U.S.A.)*

(Received July 19th, 1971)

SUMMARY

1. Mica sheets were made into membranes by a process of bombardment with fission fragments from a $U^{235}$ source and subsequent etching with hydrofluoric acid. Pores formed by this process were essentially straight through the membrane, extremely uniform in size and elliptical in cross-section. On eight of these membranes, with pore radii ranging from 45 to 300 Å, air flow, water flow, and diffusion rates for a graded series of 7 solutes were measured. From measurements of the diffusion rate of mostly non-electrolytes, with radii between 2.5 and 22.5 Å, the true hindrance effect on diffusion within pores was determined.

2. Restriction of diffusion for even relatively small solutes is a very significant effect and can be adequately described by the Renkin equation $\mathscr{D}_m/\mathscr{D}_0 = (1-R_s/R_p)^2 \times (1-2.104\ R_s/R_p + 2.09\ (R_s/R_p)^3 - 0.95\ (R_s/R_p)^5)$ for membranes which have well-defined, straight through pores, where $\mathscr{D}_m/\mathscr{D}_0$ is the ratio of solute diffusivity in the membrane to that in free solution, and $R_s/R_p$ is the ratio of solute radius to pore radius. An approximation to the Renkin equation, $\mathscr{D}_m/\mathscr{D}_0 = (1-R_s/R_p)^4$, which is much simpler to use, correlates as well with the data in the range $0 < R_s/R_p < 0.2$.

3. Water flow under small pressure drops is well described by the assumption of Poiseuille flow for this range of pore diameters, and therefore no effects due to "anomalous" water were apparent.

4. In most membrane operations there is a considerable resistance to diffusion due to the presence of a liquid film boundary layer along the surface of the membrane. This boundary layer resistance was not inversely proportional to the solute diffusivity as has often been assumed in the "unstirred layer" theory, but instead was found under these experimental conditions to be proportional to the −0.6 power of the solute diffusivity.

5. Boundary layer diffusion resistances were obtained by two independent methods: an electrochemical polarographic method and a membrane substitution method using membranes of known permeability to calibrate the diffusion cell.

6. Heteroporous membranes do not differ from isoporous membranes very much in regard to the relative hindrance of solute molecules, as long as the ratio of

* Present address: Champion Paper Co., Chicago, Ill. (U.S.A.).
** To whom reprint requests should be sent.

solute radius to mean pore radius is less than 0.2. For larger solute molecules, heteroporous membranes become increasingly less effective in hindering diffusion rates through the membrane.

## INTRODUCTION

Numerous experiments on membrane diffusion processes carried out in recent decades have indicated that the permeability of certain types of membranes to a series of increasingly large solute molecules decreases much more rapidly than would be expected from the differences in diffusivity of the solutes alone. The data from some of these experiments are reported by COLLANDER[1], MICHAELIS[2], MANGOLD[3], SPANDAU AND GROSS[4], PAPPENHEIMER[5], RENKIN[6], FUCHS AND GORIN[7], and UZELAC AND CUSSLER[8].

This phenomenon, which has generally been called restricted or hindered diffusion, has been explained on the basis that the membranes contain pores whose size is of the same order of magnitude as the size of the solute molecules. In order to obtain mathematical models for restricted diffusion, the assumption is usually made that the membrane pores can be considered as sharp-edged, circular tubes running straight through the material. In previous experiments, however, this assumption is of very dubious validity since the pores were actually interstitial void spaces between randomly oriented cross-hatched fibers. The purpose of this research was to test the validity of the various mathematical models for restricted diffusion using artificially prepared membranes known to have well-defined pores of uniform cross-section which run straight through the material.

In order to avoid many of the uncertainties about membrane structure in previous experiments, novel membranes were prepared which have the above ideal properties. These membranes were made from very thin sheets of muscovite mica by a process involving nuclear irradiation and chemical etching which actually forms holes of near atomic dimensions running perpendicularly through the material[9–18]. The hole density could be controlled by varying the irradiation time while the hole size was a function of the time and condition of etching. Thus, a series of 8 mica membranes were made with mean pore diameters ranging from 90 to 600 Å and with pore densities ranging from $9 \cdot 10^8$ to $4 \cdot 10^{10}$ holes/cm$^2$.

Methods were developed by which these sheets of mica could be mounted in plastic holders and the diffusion rates of a series of relatively spherical solutes with molecular diameters ranging from 5 Å to 45 Å could be measured. A novel continuously circulating system was employed for determination of the diffusion rates. With this system, the concentration difference across the membrane can be monitored continuously by a refractometric technique.

Each membrane was characterized as to pore length, mean pore diameter, thickness, and pore density. Flow rates of air and water under small pressure drops were also measured and diameters calculated from these rates were compared with those calculated from diffusion rates. In the diffusion system employed, liquid boundary layers along the surface of the membranes made up a significant portion of the overall mass transfer resistance. The magnitude of these boundary layer resistances were measured by an electrochemical technique and from diffusion measurements on

membranes with pores large enough so that no hindrance of diffusion occurred within the membrane; corrections were then applied to find the true diffusion coefficients of solutes within the membrane pores. A preliminary report on these studies has been published earlier[19].

## PREPARATION OF MICA MEMBRANES

One of the greatest difficulties encountered in this research was the devising of techniques by which sheets of mica could be made into membranes that could be characterized as to membrane area, pore length, pore density, pore diameter, and diffusion rate. The extreme thinness (3 to 5 $\mu$m) of the mica sheets (Ashville Schoonmaker Mica Co., Newport News, Va.) makes them very fragile and subject to cracking at the slightest strain.

After considerable trial and error, it was found that the mica sheets could best be mounted on 0.04-inch-thick sheets of vinyl plastic and cemented in place with an epoxy resin (No. 2158B/A supplied by 3M Company). The epoxy was also used to repair cracks which inevitably occurred in the mica.

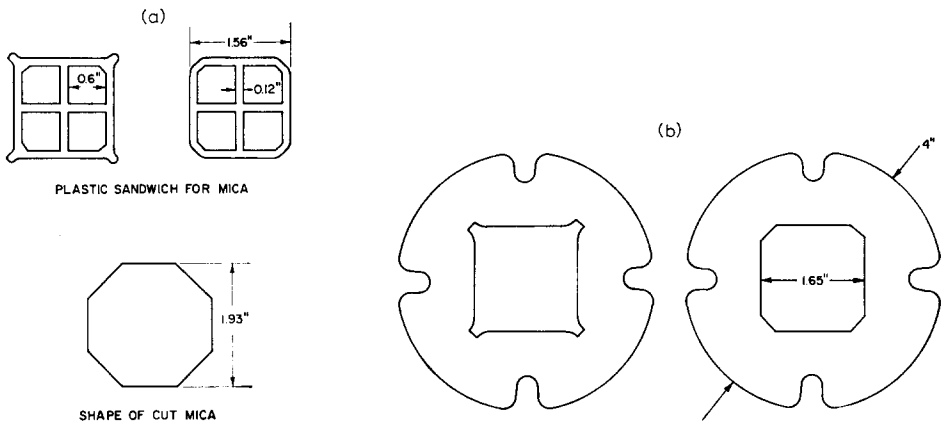


Fig. 1. (a) Design of mica holder. (b) Plastic holder for diffusion experiments. Dimensions in inches.

Fig. 1 shows the design of the plastic sandwich in which the mica sheets were mounted for irradiation and etching. The cross pieces, even though they reduce the available area, are necessary to provide sufficient support for the mica.

The procedure for making holes in the mica was essentially the same as that described by FLEISCHER *et al.*[10]. The mica, in its holder, is carefully placed at one end of the aluminum irradiation capsule shown in Fig. 2. At the other end of the capsule a thin sheet of $^{235}$U–Pd foil coated with platinum (2.5 $\mu$m thick overall) is epoxied to an aluminum disc which fits inside the capsule. The $^{235}$U foil was obtained from Brookhaven National Laboratories, Upton, N.Y.

The capsule was evacuated to a pressure of about 0.1 mm Hg to practically eliminate absorption of fission fragments by air[20]. After evacuation, the capsule was lowered down into a swimming pool nuclear reactor, and the time of irradiation was chosen to obtain the desired hole density. After neutron irradiation, the pore size was controlled by varying the time of etching with 20 % HF at room temperature.

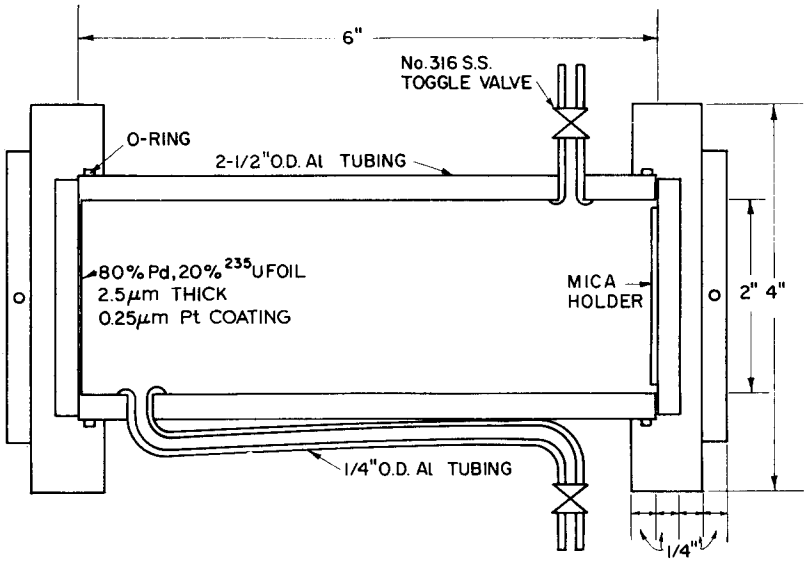


Fig. 2. Irradiation capsule. O.D. is outer diameter. Measurements in inches.

TABLE I

MEMBRANE CHARACTERISTICS

| *Membrane* | *Irradiation time (min)* | *Etching time (sec)* | *Etching temp. (°)* | *Pore length* $\times 10^4$ *(cm)* | *Pore density* $\times 10^{-8}$ $(cm^{-2})$ | *Pore radius (Å) from water flow* | *Pore radius (Å) from air flow* | *Pore radius (Å) from extrapolation* |
|---|---|---|---|---|---|---|---|---|
| Nuclepore | | | | 10.3 | 0.297 | 3275 | 4000 | |
| 33 | 10 | 100 | 40 | 4.73 | 9.17 | 306 | 322 | 292 |
| 44 | 0.67 | 420 | 25 | 4.28 | 39.7 | 119 | 115 | 110 |
| 45 | 1.5 | 500 | 25 | 4.25 | 67.5 | 172 | 171 | 166 |
| 46 | 3 | 340 | 26 | 4.42 | 66.9 | 169 | 173 | 170 |
| 47 | 15 | 150 | 25 | 3.51 | 266 | 75 | 69.5 | 74.5 |
| 48 | 10 | 120 | 26 | 3.81 | 166 | 68.5 | 62.5 | 67.5 |
| 50 | 20 | 100 | 26 | 4.40 | 370 | 58 | 55.5 | 58 |
| 51 | 20 | 70 | 26 | 4.24 | 377 | 45.7 | 38 | 44.4 |

Table I gives the etching times and resulting pore sizes for each membrane used in this study. After the etching, pieces of mica extending beyond the plastic frame were cut off for examination under an electron microscope and the plastic frame was epoxied into a larger plastic holder shown in Fig. 1 for use in diffusion, water flow, and air flow experiments.

## CHARACTERIZATION OF MEMBRANES

### *Pore length*

Pore length is one of the parameters in the diffusion equation which must be known in order to calculate solute diffusivities within the mica membranes. Because

the pores are formed by particles which pass straight through the material, the thickness of the mica quite closely approximates the mean length of the pores. This is not exactly the case, however, since in the manufacture of the membranes the source of the fission fragments making the holes was not at an infinite distance from the mica sheets. Many of the particles therefore, entered the sheets at an angle slightly less than 90° to the surface. Because of the geometry of the radiation capsule, the greatest deviation from perpendicular was 15°, or a maximum increase of 3.5 % in pore length. The proper average for the pore length at a particular location is a number average based on the number of fission particles that entered the mica surface at different angles. The mean pore length varies slightly over the mica surface, but typically the mean pore length is 1.1% greater than the thickness of the mica [21].

Membrane thicknesses were estimated by weighing a sample of known surface area, and dividing by the density of mica (2.79 g/cm$^3$). The thickness of the mica membrane decreased less than 1 % during the etching process. A similar procedure was used to estimate the thickness of Nuclepore* and Millipore* filters, the matrix density of these materials was determined to be 1.07 and 1.56 g/cm$^3$, respectively.

For the Millipore membrane, the major uncertainty in the pore length lies not in the thickness measurement but in the assumption that the thickness corresponds to the pore length (tortuosity = 1.0). Since the pore structure is unknown, it is difficult to ascertain what the tortuosity factor should be. However, because of the 75 % porosity and relatively large pore size, the tortuosity is unlikely to exceed 1.2 or 1.3 which means that the length used in calculating membrane resistances might be as much as 20 or 30% low. On the other hand, the diffusion resistances of these membranes are considerably smaller than the boundary layer resistances, and a tortuosity factor of 1.3 would decrease the estimate of the film resistances by no more than 10%. This is, by the way, the approximate difference between the estimates of boundary layer resistances from the Nuclepore and Millipore results discussed below.

*Pore density*

The pore density for each mica membrane was found by counting the number of holes in an electron micrograph of the membrane and dividing by the actual area in view (Table I).

Early indications showed that all the particle tracks were not going all the way through the mica, and care was taken to assure that only pieces from the surface away from the fission foil were collected for viewing. For each membrane, 24 electron micrographs were taken from three or four cleaved samples. In general, only a few areas (normally edges) collected on any grid were sufficiently thin and properly oriented for all the holes to be visible.

A systematic factor had to be accounted for in estimating the pore densities due to the fact that the hole density in pieces from the edge of the mica sheets used for electron micrographs differ slightly from sections in the center part used to make the membrane. An estimate of the variation in pore density is obtained by comparing the view factor from the entire $^{235}$U disc to an element of area, $\delta A$, at the center of one of the four squares in the mica holder with the view factor** from the disc to an element

* Nucleopore™, General Electric Co., Schenectady, N.Y.; Millipore™, Millipore Filter Co., Bedford, Mass.

** The view factor is the fraction of the radiation leaving one surface that intersects another surface element.

of area at the edge of the mica sheet. These view factors are $0.0267 \cdot \delta A$ and $0.0259 \cdot \delta A$, respectively and therefore, the center sections used to make membranes have a 3% higher pore density than that measured at the edges. Note that this effect cancels to some extent the increase in pore length due to particles penetrating the surface at less than 90°.

The pore density of the Nuclepore membranes was obtained from photographs of the membrane surface taken with an electron microprobe analyzer at 2500 × magnification.

*Pore shape and size distribution*

Electron micrographs of mica samples showed that the cross-sectional shape of the pore changes from oval to diamond shape with increasing etching time[10,21]. The smallest pores that have been resolved adequately by electron microscopy are about 300 Å in diameter and seem to have an oval shape[17], and therefore we assumed that the smallest pores studied here (approx. 100 Å diameter) also are oval in cross-section and can be represented mathematically as an ellipse. The ratio of the long to short axes was estimated to be about 1.5 for both the small oval and larger diamond pores, in agreement with similar measurements by BEAN[17].

The fact that the pores are not simple right cylinders introduces a slight degree of awkwardness in characterizing their size by a single number; the degree of non-circularity, however, is small and for purposes of correlation their shape can be considered circular and their size can be characterized by an equivalent circular pore diameter with little error.

Another slight non-ideality of these membranes is that all the pores in a membrane are not exactly the same size. For Membrane 48 a pore size distribution was determined from photographic enlargements of several electron micrographs, and is presented in Fig. 3. The distribution is relatively narrow with better than 80 % of the pores having diameters between 110 and 150 Å. The mean number average diameter calculated for this distribution is 133.1 Å with a standard deviation of 17.6 Å. This narrow pore size distribution compares well with other materials of controlled pore size in this size range, such as porous glass[22].

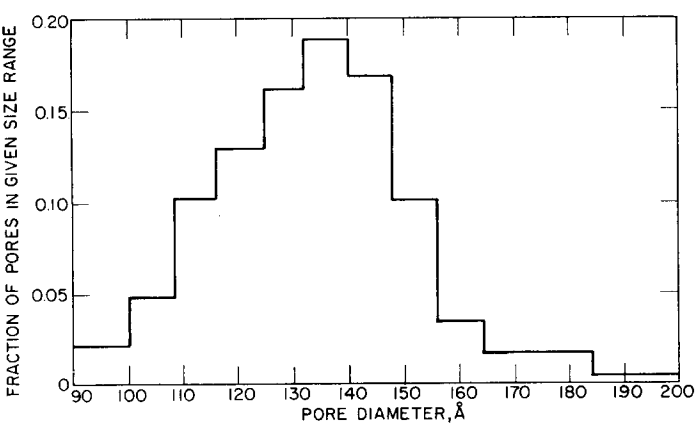


Fig. 3. Pore size distribution for Membrane 48.

*Pore size*

Although electron micrographs of the mica membranes showed that the pores were of rather uniform size, pore dimensions could not be estimated by this method with sufficient precision to obtain a value for the total pore cross-sectional area and mean diameter. Instead, fluid flow through the porous membranes was used to evaluate a mean pore size.

One of the most widely used indirect methods for estimating membrane pore diameters is through the measurement of water flow rates under an applied hydrostatic pressure. HITCHCOCK[23] in 1926 was one of the first to employ this method. For a series of collodion membranes, he measured water flow rate, porosity, and thickness, and assumed that; (1) flow through the pores was laminar with no slippage at the walls and therefore followed Poiseuille's law, (2) the measured thickness corresponded to the length of the flow channels, and (3) all volume occupied by water within the membrane was available for flow.

Noting that assumptions 2 and 3 above are not likely to be valid for membranes consisting of randomly oriented cross-hatched fibers which might absorb water into the fibers, PAPPENHEIMER[5] proposed the following equation to overcome these difficulties:

$$R_p = \left[\frac{8Q_w\mu}{\Delta P(A_0/L)}\right]^{1/2} \tag{1}$$

where $R_p$ is pore radius, $(A_0/L)$, the total open area of pores divided by the mean path length, is determined from measurements of the diffusion rate of isotopic water through the membrane, $Q_w$ is the water flow through the membrane, $\mu$ is viscosity, and $\Delta P$ is the pressure difference across the membrane.

One major difficulty with this method is that the presence of diffusion boundary layers at the surface of the membrane can cause large errors in the calculation of $(A_0/L)$ but have no effect in the water flow measurements. If uncorrected, pore diameters are calculated which are considerably higher than the true value.

A question arises as to the validity of the Poiseuille flow assumption as the pore size approaches that of the water molecules. Obviously, for pores of the same order of magnitude as the molecular diameter of water, the transport mechanism cannot be laminar flow, but instead must be diffusional. There is some controversy as to where the transition occurs. KEDEM AND KATCHALSKY[24] report that the mechanism is primarily laminar flow for pores as small as 20 Å. KOEFFED-JOHNSON[25] concurs. LAKSHMINARAYANAIAH[26] on the other hand, claims that flow is primarily laminar for 70 Å pores but is primarily diffusional for 20 Å pores. BEAN[17] in studies on water flow through micro-porous membranes simultaneous with, but independent of, the work presented here finds, as we do, no evidence for anomalous flow behavior for pores larger than 60 Å in diameter.

Flow rates of water through each mica and Nuclepore membrane were measured under a small pressure head with the apparatus shown in Fig. 4. This apparatus contained the membrane holder of Fig. 1 which was placed between two water reservoirs. A 2-ml syringe was used to increase the volume of the downstream side until the meniscus indicated the desired pressure difference between the two chambers, generally 8 cm.

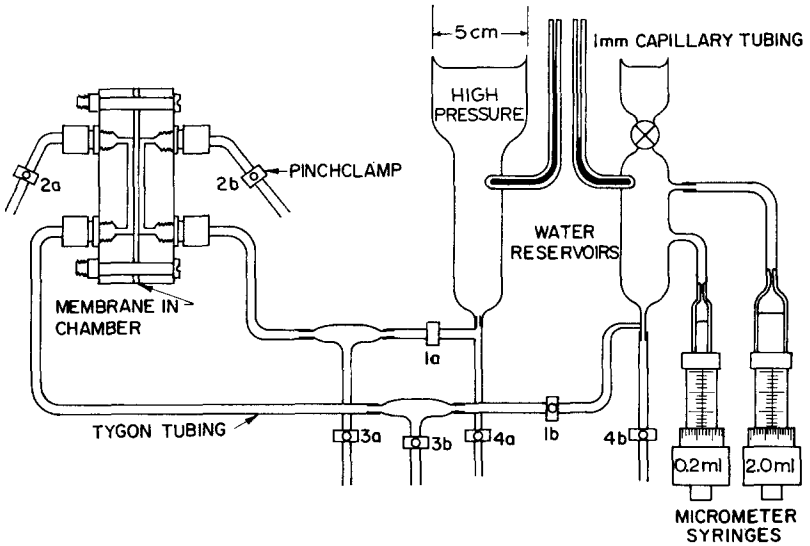


Fig. 4. Water flow apparatus for determining the pore size in membranes.

TABLE II

AIR FLOW AND WATER FLOW DATA

| *Membrane* | $(Q_a/\Delta H) \times 10^2$ *(ml/cm·sec)* | $(Q_w/\Delta H) \times 10^5$ *(ml/cm·sec)* |
|---|---|---|
| Nuclepore | 140 | |
| 33 | 1.018 | 1.363 |
| 44 | 0.640 | 0.352 |
| 45 | 3.367 | 3.17 |
| 46 | 3.433 | 2.38 |
| 47 | 1.135 | 0.550 |
| 48 | 0.583 | 0.197 |
| 50 | 1.025 | 0.287 |
| 51 | 0.338 | 0.125 |

The change in volume of a 0.2-ml syringe, read to the nearest 0.0001 ml in a timed period gave the water flow rate for the set pressure difference.

In order to calculate pore diameters from the measured water flow rates given in Table II, Poiseuille flow through the pores was assumed. The rate of laminar flow, $Q_w$, through tubes with elliptical cross-section is given by:

$$Q_w = n_0 A_m \frac{\pi \Delta P}{4\mu L} \frac{a^3 b^3}{(a^2 + b^2)} = n_0 A_m \frac{\pi \Delta P}{4\mu L} a^4 \left( \frac{\alpha^3}{1 + \alpha^2} \right) \quad (2)$$

where $a$ and $b$ are the lengths of the major and minor axes, and $\alpha = b/a$. $n_0$ is the number of pores per unit area of membrane, $A_m$ is the area of membrane, $\Delta P$ is the pressure difference, $\mu$ is the fluid viscosity, and $L$ is the pore length.

The radius of an equivalent circular pore can be defined in two ways, either as the radius of the circular tube that gives the same flow, $R_{pf}$, or the radius of the circular pore that gives the same cross-sectional area, $R_{pd}$. If diffusion within the pore is unhindered then $R_{pd}$ is also the radius for the circular pore that gives the same diffusion rate as the ellipse. The two definitions for equivalent pore radius are calculated from:

$$R_{pf} = a\left(\frac{2\alpha^3}{1+\alpha^2}\right)^{1/4} \tag{3a}$$

$$\pi R_{pd}^2 = \pi ab; \quad R_{pd} = a\alpha^{1/2} \tag{3b}$$

where $a$ is calculated from flow measurements using Eqn. 2 above. The ratio $R_{pd}/R_{pf}$, which is exactly one for circular pores, gives a measure of the error incurred in assuming the elliptical pores in these membranes are circular

$$\frac{R_{pd}}{R_{pf}} = \left(\frac{1+\alpha^2}{2\alpha}\right)^{1/4} \approx 1.02 \tag{3}$$

where $\alpha = 1/1.5$ for the mica membranes.

In the treatment of data for estimating hindered diffusion effects, $A_d$, the total cross-sectional pore area was calculated from

$$A_d = n_0 A_m \pi ab = \left[n_0 A_m \pi \left(\frac{Q_w 4\mu L}{\Delta P}\right)\left(\frac{1+\alpha^2}{\alpha}\right)\right]^{1/2} \tag{4}$$

and the pore size was characterized by the effective pore radius for diffusion, $R_{pd}$, as defined above.

$$R_{pd} = a\alpha^{1/2} = \left[\left(\frac{Q_w 4\mu L}{n_0 A_m \pi \Delta P}\right)\frac{(1+\alpha^2)}{\alpha}\right]^{1/4} \tag{5}$$

The equivalent pore radius of each membrane calculated in this fashion from water flow data is listed in Table I. The close agreement of pore radii by the water flow method with radii determined by other means demonstrates the validity of the Poiseuille flow assumptions even for flow in tubes of close to molecular dimensions.

Flow rate of air through each of the mica membranes was measured with the apparatus shown in Fig. 5. The experimental procedure was as follows: the membrane in its plastic holder was bolted between two lucite chambers; as air was forced into the chamber, the pressure, as measured by the water manometer, rose until air flowed (or diffused) through the membrane at the same rate at which it was being forced in by the syringe pump. The flow rates which could be used were limited by the fact that no more than 10 to 12 cm water pressure drop could be safely applied across the mica without taking the risk of cracking it. Based on approximate values for the pore diameters and the nearly atmospheric gas pressure, it could be shown that air flow through the pores in the mica membrane was in the Knudsen flow regime[21].

The air flow data given in Table II are the mean values of approximately 10 determinations of each membrane. Pore diameter estimates were based on the assump-

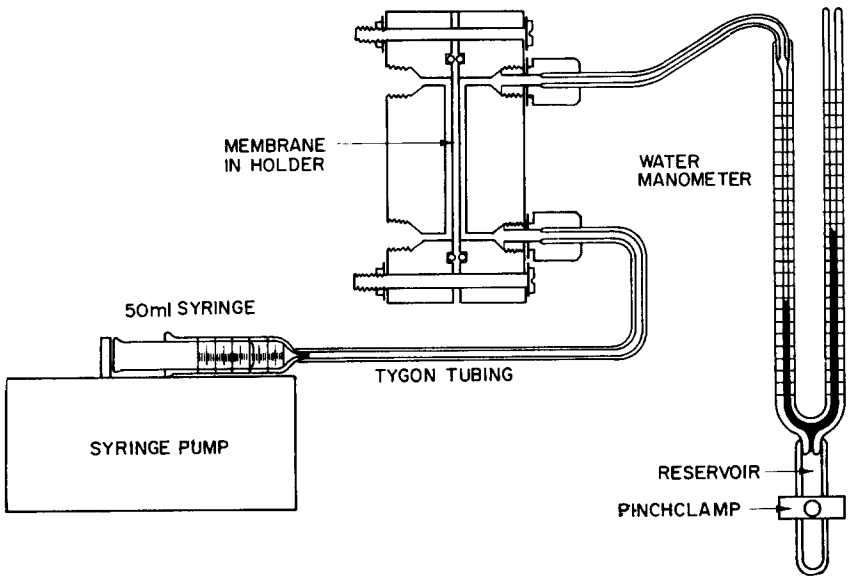


Fig. 5. Air flow apparatus for determining the pore size in membranes.

tion of Knudsen diffusion, which predicts a third power dependence of flow on pore diameter. For the experimental apparatus described here, the Knudsen equation becomes:

$$R_p^3 = \frac{(1033\, P_{atm} + \Delta H) L Q_a}{34 \times 10^4\, n_0 A_m \sqrt{T}\, \Delta H} \tag{6}$$

Where $P_{atm}$ is the barametric pressure, $\Delta H$ is water pressure head across the membrane, and $T$ is the absolute temperature.

It can be seen from the next to the last column in Table I that the radii calculated from Eqn. 6 are in very good agreement with the water flow radii for Membranes 44, 45, 46, and 50. It is difficult to place much significance on the deviations observed for No. 33 and the Nuclepore membrane. For these, the flow rates were so high that, with the apparatus used, it was impossible to measure the air flow rates with any degree of accuracy.

Pore radii by the air flow method for the last 4 membranes are significantly lower than the water flow and diffusion radii. For Membrane 51, and assuming Knudsen flow, the air flow rate was 40% lower than would be predicted from the water flow method. It is uncertain, however, if this indicates a lack of applicability of the Knudsen diffusion assumption for the smaller pores. Fok *et al.*[27], have demonstrated that clean surfaces of mica can adsorb water from the air to form a film as much as 80 Å thick. The low values of the air flow diameters for these membranes could therefore be due to a one or two molecule thick layer of adsorbed water on the surface of the pores.

As mentioned previously, electron micrographs indicate that there is a distribution of pore radii in each membrane. Neglecting hindered diffusion effects for the moment, the means of this distribution weighted according to the square, cube, and fourths

power of the pore radius gives the magnitude of the differences that might be expected between the water flow, air flow, and diffusion methods which can be attributed to the pore size distribution. The means calculated in this manner for Membrane No. 48 show very little difference, indicating that the pore size distribution had a relatively minor effect in these studies.

$$R_{p\,\mathrm{mean}}^{2} = \sqrt{\Sigma \frac{n_i R_i^2}{n_t}} = 67.3 \text{ Å}$$

$$R_{p\,\mathrm{mean}}^{3} = \sqrt[3]{\Sigma \frac{n_i R_i^3}{n_t}} = 67.8 \text{ Å}$$

$$R_{p\,\mathrm{mean}}^{4} = \sqrt[4]{\Sigma \frac{n_i R_i^4}{n_t}} = 68.4 \text{ Å}$$

## DIFFUSION EXPERIMENTS

### *Choice of solutes*

In order to measure restriction to diffusion for a range of values of the ratio of solute size to pore size, it was necessary to choose a series of solutes of increasing size. The criteria for choice were: (1) the molecule should have a relatively spherical rather than long-chain conformation, (2) the compounds should be attainable in high purity from commercial sources, (3) they should cover a wide range of molecular diameters, and (4) they should be relatively common compounds whose diffusivities in free solution have been previously measured[49].

On this basis, the following compounds were selected: urea, glucose, sucrose, raffinose, α-dextrin, β-dextrin, and ribonuclease. The Schardinger dextrins, also known as cyclohexaamylose and cycloheptaamylose, are ring sugars containing 6 and 7 glucose units, respectively. As such, they have disc conformations with diameters of approximately 16 Å and 17 Å and heights of about 9 Å[28].

Baker reagent grade urea, glucose, sucrose, and raffinose were used without any further purification. The Schardinger dextrins and the ribonuclease were obtained from Pierce Chemical Company, Rockford, Ill. The α-dextrin had to be released from a cyclohexane complex by a recrystallization process described by FRENCH[28].

In order to avoid system contamination by oily or particulate matter or by bacteria growth in the sugar solutions, all test solutions were made up in a well-cleaned 100-ml volumetric flask just prior to each run. For all solutes except ribonuclease, ordinary distilled and filtered water was used. Ribonuclease solutions were brought to the isoelectric point, pH 7.8, with small amounts of $Na_2CO_3$ solution.

There is some controversy as to the radii of these solutes that best characterizes their apparent size in water solution. It was decided that the most accurate radii to use for this purpose is that calculated from the free diffusivity by means of the Stokes–Einstein equation

$$R_{s\mathrm{E}} = RT/6\pi\mu\mathscr{D}_0 N_{\mathrm{Av}} \tag{7}$$

where $R_{s\mathrm{E}}$ is the Stokes–Einstein solute radius, $R$ is the gas constant, $T$ is absolute temperature, $\mu$ is viscosity, $\mathscr{D}_0$ is the diffusivity in free solution, and $N_{\mathrm{Av}}$ is Avogadros

number. A correction, derived by GIERER AND WIRTZ[29], to account for the fact that the solute molecule has a size comparable to that of a water molecule was applied. This correction is:

$$R_s = \left(1.5R_w/R_s + \frac{R_s}{R_s + 2R_w}\right) R_{sE} \tag{8}$$

and can be solved by successive approximations; where $R_s$ is the equivalent solute radius used in this study and $R_w$, the radius of a water molecule, is approximately 1.5 Å according to ORRTUNG[30]. Table III gives the diffusivities and solute radii used in this study. The final column gives the literature source for the free diffusivity.

TABLE III

SOLUTE PROPERTIES

| *Solute* | $\mathscr{D}_0 \times 10^6$ ($cm^2/sec$) | $R_s$ (Å) | *Source* |
|---|---|---|---|
| Urea | 13.8 | 2.64 | LONGSWORTH[48] |
| Glucose | 6.73 | 4.44 | LONGSWORTH[48] |
| Sucrose | 5.21 | 5.55 | LONGSWORTH[48] |
| Raffinose | 4.34 | 6.54 | LONGSWORTH[48] |
| α-Dextrin | 3.44 | 8.00 | CRAIG[49] |
| β-Dextrin | 3.22 | 8.98 | CRAIG[49] |
| Ribonuclease | 1.18 | 21.6 | JOUBERT AND HAYLETT[50] |

*Design of apparatus*

The equation describing the diffusion through a membrane separating two closed compartments has been given earlier[3]:

$$\ln \frac{\Delta C}{\Delta C_0} = \frac{A_m}{R_0}\left(\frac{1}{V_1} + \frac{1}{V_2}\right) t = S \cdot t \tag{9}$$

where $\Delta C$ is the concentration difference between the two mixed chambers at any time, $t$, after initiating the experiment. $\Delta C_0$ is the initial concentration difference, $A_m$ is the membrane area, $R_0$ is the overall resistance of the membrane and boundary layer*, and $V_1$, $V_2$ are the chamber volumes. In the development of this equation it is implicit that there is no bulk fluid flow through membrane due to hydraulic or osmotic pressure differences. The slope of a plot of ln $\Delta C$ *vs.* time gives the proportionality constant, $S$, directly.

Basically, the apparatus shown in Fig. 6 worked as follows: fluid in the glass standpipe, fashioned from a 10 ml graduated pipette with a widened top and a glass tubing inlet attached in the middle, was continuously recirculated through a rotameter to the diffusion chamber and back to the standpipe. The two halves of the system were made as identical as possible. The total liquid volumes on each side of the membrane were 39.2 ± 0.3 ml including 6.2 ml for each refractometer circuit. The

* In this paper we will often refer to resistances to diffusion, in analogy to electrical terminology. Please note that the resistance of a layer to diffusion is exactly equivalent to the inverse of the effective permeability of that layer, *e.g.* $R_0 = 1/P_0$.

design of the diffusion chamber is shown in Fig. 7. The cell, pumps, and standpipes were kept within a constant temperature bath maintained at 25.0° ± 0.1°.

From the high pressure side of the pumps, fluid was forced up to other standpipes made from 1/8 inch inner diameter polyethylene tubing. From there, solutions flow by gravity through the differential refractometer (Waters Instrument Company), where the concentration difference was monitored and recorded, and back into the main system. Overflow lines were provided in order to maintain a constant liquid level in the polyethylene standpipes, and thereby constant flow of about 1.5 ml/min through the differential refractometer.

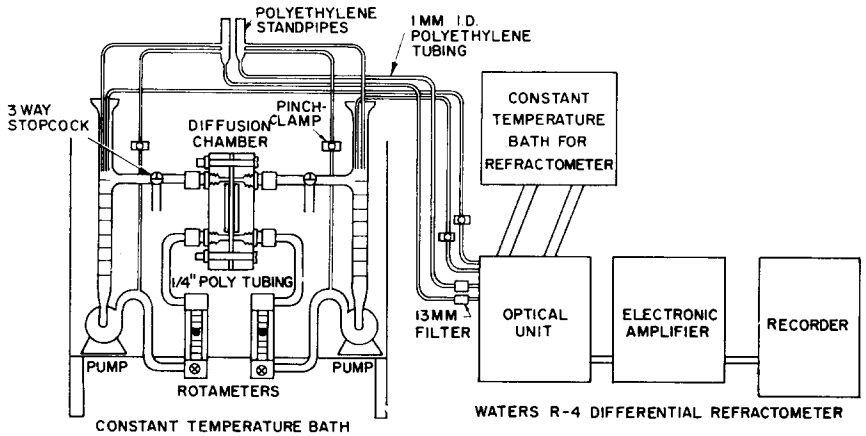


Fig. 6. Apparatus for diffusion measurements across membranes. I.D. is internal diameter. Dimension of polytubing measured in inches.

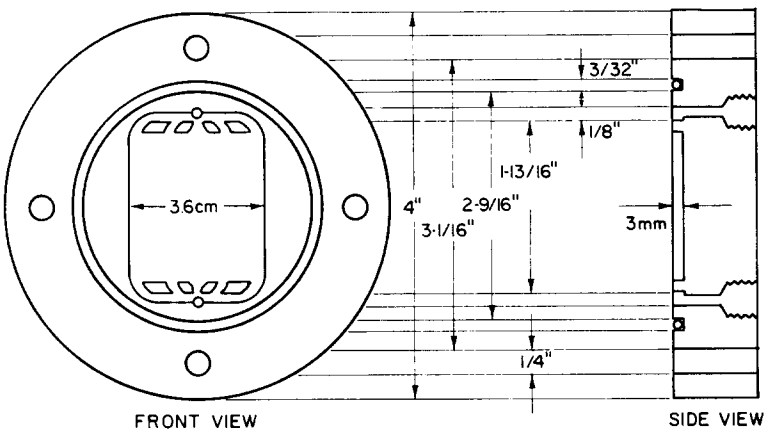


Fig. 7. Diffusion chamber. Diameter measurements in inches.

It might be supposed that the hold-up of solution flowing slowly through the refractometer circuit would cause the diffusion rate as measured from the refractometer chart readings to differ appreciably from the true diffusion rate across the membrane. However, an analysis of this problem[21] indicates that the flow rate through the

refractometer is sufficiently high compared to the diffusion rates so that, even for the most permeable membrane, the error is less than 0.3 %.

In the range of solute concentrations used here, 0 to 0.06 wt. %, refractive index is directly proportional to solute concentration and the output of the instrument is a direct measure of the concentration difference between the two solutions flowing through the optical cell. The instrument, when operated properly, is sensitive enough to detect a concentration difference of one part per million.

An interesting aspect of the refractometry is that the chart reading is approximately the same for all the compounds tested on a weight percent basis. That is, a 0.05 % solution of urea will give about the same reading when compared to pure water as will a 0.05 % solution of $\beta$-dextrin, although in the former case there are nearly 20 times as many molecules per unit volume as in the latter.

*Boundary layer effects*

In order to find the diffusivity of solutes in the microporous membrane it is necessary to know the geometrical dimensions of the membrane pores as well as the concentration difference of solute directly across the membrane solution interface. The solute concentration difference across the membrane alone is difficult to measure directly and usually has to be inferred from measurements of concentration at some distance from the interface of the membrane.

There are several experimental configurations which allow one to calculate the solute concentrations at the membrane interface from a detailed knowledge of the fluid flow in the region of the membrane interface. Configurations such as flow over a flat plate, flow to rotating discs, and laminar flow in tubes are susceptible to exact mathematical analyses of the boundary layer resistance to diffusion[31]. However, because of the fragility of the mica membranes and experimental considerations requiring small volumes of solutions, our diffusion apparatus could not be made to conform to any of the above flow systems.

We therefore elected to measure experimentally the boundary layer resistance to solute diffusion, $R_f$. Then with a measurement of the overall diffusion resistance for a particular solute–membrane combination, concentrations at the membrane surfaces or the equivalent membrane resistance, $R_m$ were calculated by Eqn. 12.

Two methods were used to estimate boundary layer contributions to the overall diffusion resistance between the solutions on both sides of the membrane. An electrochemical technique based on polarography was used to estimate the boundary layer resistance at various flow rates. The technique involves the oxidation of $Fe(CN)_6^{4-}$ to $Fe(CN)_6^{3-}$ at the surface of a platinum electrode over which an electrolytic solution of the two is flowing. As the applied voltage is increased, a point is reached at which the concentration of $Fe(CN)_6^{4-}$ is essentially zero at the surface of the platinum electrode and the measured limiting current, $i_L$, is directly related to the mass transfer coefficient, $k_c$, for the liquid film along the electrode[32]. The mass transfer coefficient for $Fe(CN)_6^{4-}$ in the system was calculated from the following equation:

$$k_c = i_L/nFAc_B \tag{10}$$

where $n$ is the number of equivalents per mole of reactant, $F$ is Faraday's constant, $A$ is the electrode area, and $c_B$ is the bulk concentration of the reactant.

Fig. 8 shows the apparatus used for this measurement. The mass transfer

coefficient is related to the boundary layer resistance by $k_c = 1/R_f$ and is known to be a function of solute diffusivity as well as other properties of the fluid[33].

In order to duplicate flow conditions as closely as possible, the plastic electrode holder was made identical to the membrane holders. Into one of the squares, a sheet of smooth platinum was epoxied to serve as the working electrode. Into another

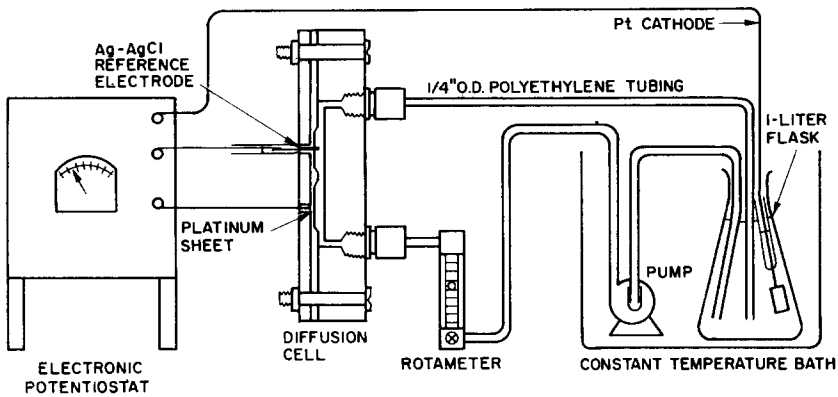


Fig. 8. Electrochemical apparatus for measuring diffusion resistance of liquid boundary layers near the surface of a membrane. O.D. is outer diameter, measured in inches.

of the squares was inserted the tip of a Ag–AgCl reference electrode. This holder was then clamped between one-half of the flow cell used for diffusion studies and a lucite backing plate. The electrolyte consisted of a solution containing 0.01 M $K_3F_6(CN)_4$, 0.01 M $K_4Fe(CN)_6$, and 0.5 M $K_2SO_4$. Temperature was maintained at 26° and the limiting current $i_L$, was measured at each of 8 rotameter settings for each of the four possible orientations of the square platinum electrode.

Many studies in the engineering literature have shown that mass transfer data can be normalized by converting the data into a dimensionless form[33]. The commonly used dimensionless groups are the Stanton number, $St = k_c/u_\infty$; the Reynolds number, $Re = R_H u_\infty \rho/\mu$; and the Schmidt number, $Sc = \mu/\rho\mathscr{D}_0$. Where $k_c$ is the mass transfer coefficient; $u_\infty$ is the bulk fluid velocity; $R_H$ a typical dimension for the system such as the radius of the flow channel; $\mu$ and $\rho$ the kinematic viscosity and density of the fluid; and $\mathscr{D}_0$ the diffusivity of a solute.

TABLE IV

ELECTROCHEMICAL MASS TRANSFER RESULTS

| $u_\infty$ (cm/sec) | $k_c \times 10^3$ (cm/sec) | $St \times 10^4$ | $Re$ | $St\ Sc^{0.6}$ |
|---|---|---|---|---|
| 1.33 | 0.78 | 5.78 | 121 | 0.0535 |
| 2.02 | 1.01 | 5.00 | 183 | 0.0456 |
| 2.70 | 1.20 | 4.45 | 245 | 0.0406 |
| 3.18 | 1.32 | 4.16 | 289 | 0.0379 |
| 3.38 | 1.40 | 4.14 | 307 | 0.0377 |
| 4.06 | 1.56 | 3.85 | 368 | 0.0351 |
| 4.74 | 1.68 | 3.55 | 420 | 0.0323 |
| 5.42 | 1.80 | 3.32 | 492 | 0.0302 |

Mass transfer coefficients for varying bulk velocities were calculated from measured limiting currents using Eqn. 10, Table IV. Visual observations indicated that the flow regime within the chamber was turbulent throughout this range of velocities. In order to obtain an averaging of the data and to test a correlation of the form of $St = f(Re, Sc)$, the product $StSc^{0.6} = (k_c/u_\infty)(\nu/\rho\mathscr{D}_0)^{0.6}$ was plotted against the Reynolds number as shown in Fig. 9.

The diffusivity of $K_4Fe(CN)_6$ was reported as $5.0 \cdot 10^{-6}$ cm²/sec by JAHN AND VIELSTICH[34] for this test solution. The —0.6 dependence of the Stanton number on the Schmidt number was incorporated from membrane diffusion results with macroporous membranes reported below. Using the slope and intercept of the line through the data points yields the correlation:

$$St = 0.35Sc^{-0.6}Re^{-0.4} \tag{11}$$

Although the electrochemical method is easily adaptable to finding the effect of flow on diffusion through the boundary layer, the effect of varying solute diffusivities is not as easily revealed by this method because of the lack of electroactive solutes over a wide range of molecular weights.

We therefore elected to estimate the variation in boundary layer resistance with solutes by measuring the overall diffusion resistance at the same flow as used with the mica membranes but with membranes of known permeability. For a given solute and flow past the membrane, the relationship between membrane permeability and mass transfer coefficient in the boundary layers can be represented by:

$$R_0 = R_m + 2R_f \tag{12}$$

We have assumed that the experimental apparatus is symmetrical so that the boundary layer resistance is equal on both sides of the membrane and $R_f$ represents

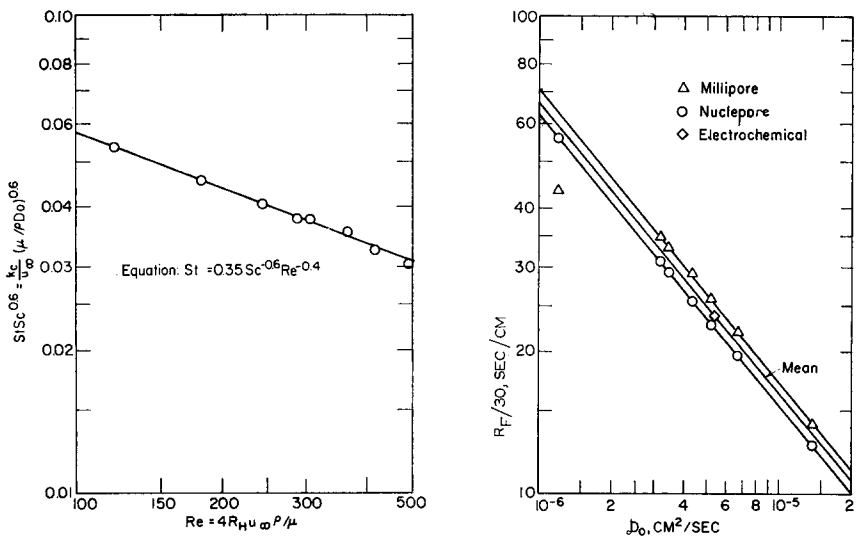


Fig. 9. Mass transfer coefficients (boundary layer resistances) measured by an electrochemical method, as a function of the fluid velocity across the membrane surface.

Fig. 10. Boundary layer diffusion resistance as a function of solute diffusivity.

one of these two resistances. The overall resistance and mass transfer $R_0$ is calculated from the changes in solute concentrations within the chambers with time (Eqn. 9); if the permeability of the membrane ($1/R_m$) is known independently, then $R_f$ can be calculated directly. In addition, in the particular circumstance of diffusion through membranes, the mass transfer coefficient, $k_c$, may be a function of membrane permeability, $P_m$ (SMITH *et al.*[35], BABB *et al.*[36]). These authors have calculated $k_c$ as a function of the ratio $P_m/k_c$ or $R_f/R_m$ (wall Sherwood number) for laminar flow mass transfer devices. In the case of laminar flow over a membrane in a rectangular channel[36] the maximum variation of $k_c$ over the complete range of possible values of $P_m$ is about 10%. Even though the apparent Reynolds number in our diffusion cell was about 300, which would place the experiments in the laminar regime, observation of the flow pattern showed that the flow was actually turbulent. This was due to the jet-like orifices in the entry to the diffusion cell.

Corresponding theory for calculating the effect of wall Sherwood number on mass transfer coefficients in turbulent flow has not been developed, but one would expect that the magnitude of the effect to be of the same order as in the laminar region, *i.e.* less than 10%. Therefore, this effect is ignored here in evaluating the magnitude of the boundary layer resistance from diffusion studies with membranes of known permeability.

Diffusion experiments were conducted with a Nuclepore and Millipore membrane whose porosity and thickness were measured as previously described. Since these membranes have pore sizes on the order of 4000 Å, it could be assumed that there was no appreciable restriction to diffusion for any of the solute molecules. With no restriction, the expected membrane resistance is just the pore length divided by the product of the porosity and the free diffusivity.

Table V gives the resistances determined from diffusion measurements on a Nuclepore and a Millipore membrane. These resistances were calculated as follows:

$$R_0 = A_m(1/V_1 + 1/V_2)/S \tag{13a}$$

$$R_m = L/\pi n_0 \mathscr{D}_0 R_p^2 \text{ for Nuclepore} \tag{13b}$$

$$R_m = L/\mathscr{D}_0 \text{ for Millipore} \tag{13c}$$

$$R_f = (R_0 - R_m)/2 \tag{13d}$$

By the methods previously described, the Millipore membrane was found to have a porosity of 0.73 and a thickness of 26 $\mu$m (nominal values are 0.8 and 25 $\mu$m. The pore diameters used for the Nuclepore membranes were those determined from water flow data reported in Table II.

It is quite possible that the thickness of the Millipore membrane does not correspond to the diffusion path length for the solutes. The high porosity of the membrane, however, suggests that the difference should not be large. Moreover, since the membrane resistance in this case makes up only a small part of the overall resistance, the resulting percentage error in the calculated film resistance will be considerably smaller than the percentage error in the path length. For instance, an error of 20% in the path length would lead to only a 6% error in the estimation of the film resistance.

TABLE V

DIFFUSION RESULTS FOR PLASTIC MEMBRANES

| *Solute* | *Overall resistance* $R_0 \times 10^{-2}$ *(sec/cm)* | *Membrane resistance* $R_m \times 10^{-2}$ *(sec/cm)* | *Boundary layer resistance* $R_f \times 10^{-2}$ *(sec/cm)* |
|---|---|---|---|
| | *Nuclepore 3* | | |
| Urea | 15.12 | 7.50 | 3.81 |
| Glucose | 27.12 | 14.76 | 5.88 |
| Sucrose | 33.42 | 17.94 | 6.74 |
| Raffinose | 39.24 | 23.94 | 7.65 |
| α-Dextrin | 47.64 | 30.06 | 8.79 |
| β-Dextrin | 50.58 | 32.10 | 9.24 |
| Ribonuclease | 126.0 | 92.4 | 16.8 |
| | *Millipore 1* | | |
| Urea | 10.95 | 2.58 | 4.18 |
| Glucose | 18.42 | 5.28 | 6.57 |
| Sucrose | 22.38 | 6.84 | 7.77 |
| Raffinose | 25.62 | 8.22 | 8.70 |
| α-Dextrin | 30.00 | 10.32 | 9.84 |
| β-Dextrin | 31.98 | 11.04 | 10.47 |
| Ribonuclease | 55.92 | 29.88 | 13.02 |

Fig. 10 demonstrates that plots of the boundary layer film resistance *versus* diffusivity on a log–log scale gave excellent straight lines. The slope of each of these lines is approximately —0.6, indicating that the presence of the film resistance could not be viewed as arising from a "stagnant liquid film" of constant thickness[51].

The stagnant film theory would predict that $R_f$ is inversely proportional to the diffusivity, $\mathscr{D}_0$ of the diffusing molecule, *i.e.* in a plot of $R_f$ *vs.* $\mathscr{D}_0$ the slope would be —1.0. The experimental evidence given here shows conclusively that the stagnant film theory must be used with caution in correcting overall permeability measurements to obtain true membrane permeabilities. Errors may be especially significant if the "film thickness" is determined with a solute of much different diffusion coefficient than another solute of interest. For example, if the boundary layer resistance for a membrane is determined with isotopically labelled water, but the solute of actual interest is glucose, then the estimated membrane permeability for glucose by the stagnant film theory may be in serious error. The magnitude of the error depends of the relative magnitude of the boundary layer resistance to diffusion as compared to the resistance of the membrane alone.

Our experimental observations on mass transfer coefficients estimated by both the electrochemical and known permeability methods give very similar estimates of the boundary layer mass transfer coefficients.

The film resistance expected if $K_4Fe(CN)_6$ were used in the membrane diffusion experiments can be calculated and compared with Fig. 10. All membrane diffusion experiments were made at a rotameter setting of 4.7 (the maximum possible in the diffusion apparatus). This corresponds to a velocity of 3.18 cm/sec and a Reynolds number of 296. From Fig. 9 at this value of *Re*, $StSc^{0.6} = 3.78 \cdot 10^{-2}$; $Sc = 1680$, and $Sc^{0.6} = 86.0$. Then $St = k_c/u_\infty = 4.40 \cdot 10^{-4}$ and $k_c = 1.40 \cdot 10^{-3}$ cm/sec.

Converting to the proper units and noting that in the diffusion experiments there are identical films on each side of the membrane, for $\mathscr{D}_0 = 5.35 \cdot 10^{-6}$ cm²/sec (in a solution with the approximate viscosity of pure water at 25°), $R_f = k_c^{-1} = 714$ sec/cm.

This point falls midway between the Millipore and Nuclepore results in Fig. 10 and therefore adds considerable confidence to the use of the mean of these results which are tabulated in Table VI and assumed to be valid for the diffusion experiments with mica membranes. These data indicate that under our conditions, the mass transfer coefficient is relatively independent of membrane permeability.

A series of experiments were also carried out to learn more about the uniformity

TABLE VI

AVERAGE BOUNDARY LAYER RESISTANCES OF SOLUTES

| *Solute* | $\mathscr{D}_0 \times 10^6$ (*cm²/sec*) | *Rf* (*sec/cm*) |
|---|---|---|
| Urea | 13.8 | 402 |
| Glucose | 6.73 | 620 |
| Sucrose | 5.21 | 730 |
| Raffinose | 4.34 | 815 |
| α-Dextrin | 3.44 | 950 |
| β-Dextrin | 3.22 | 990 |
| Ribonuclease | 1.18 | 1800 |

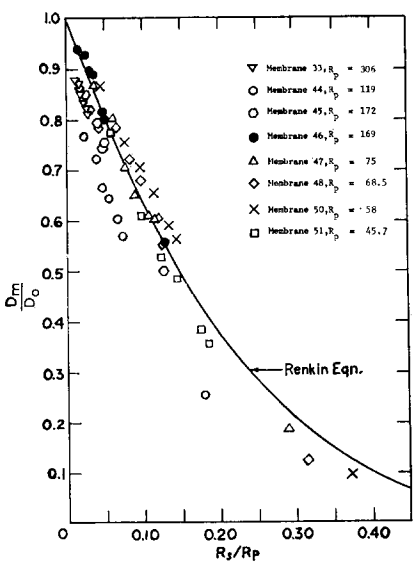


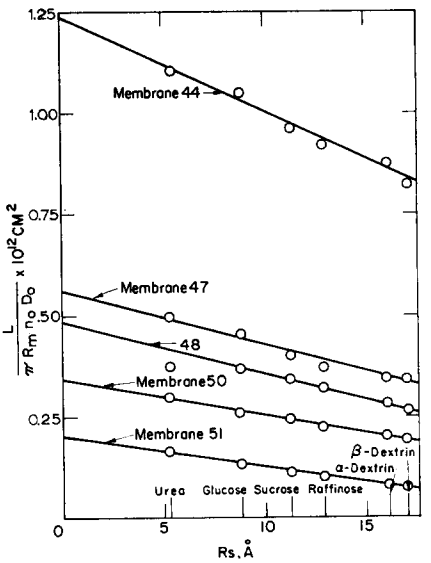


Fig. 11. Ratio of solute diffusivity in membrane pore to solute diffusivity in free solution, $\mathscr{D}_m/\mathscr{D}_0$, as a function of the ratio of solute radius to pore radius, $R_s/R_p$. Pore radius determined from water flow measurements.

Fig. 12. Extrapolation of diffusion data for membranes to obtain an estimate of the pore size in membranes.

of the boundary layer resistance over the membrane surface. The Nuclepore membrane was constructed with a plastic crosspiece in the middle leaving the exposed membrane area in the form of two rectangles approximately 1.3 cm by 2.9 cm. Diffusion runs with the rectangles in vertical and horizontal positions showed no difference in the liquid film resistances. Therefore, the plastic crosspiece had no effect on the boundary layer resistance, which is additional evidence that flow was not laminar in the diffusion cell.

As a further check, one of the rectangles was filled with epoxy, and the diffusion rates for urea were measured for three orientations of the other rectangle: horizontally in the lower part of the chamber, vertically, and horizontally in the upper part. Boundary layer resistances corresponding to these three orientations were 288, 372, and 447 sec/cm. The most probably explanation for these results is that the degree of turbulence is much greater in the inlet section of the chamber than in the exit section.

These results were confirmed in the electrochemical mass transfer coefficient experiments. Determinations of $k_c$ were made for the square platinum electrode in its four possible orientations. For the lower part of the chamber, the mean film resistance for $K_4Fe(CN)_6$ was found to be 636 sec/cm and for the upper part, 927 sec/cm. The ratio of the lower resistance to the upper of 0.68 agrees well with the ratio of 0.65 found with the Nuclepore membrane.

## RESULTS

### *Restricted diffusion*

The diffusion rates of each of the test solutes given in Table VII were measured through mica membranes with pore sizes in the range of 100–600 Å. These data give a rather complete coverage of possible combinations of pore size and molecular size. In each experiment, diffusion between the two chambers was allowed to proceed until the solute concentration difference between the chambers was about one-half the initial value. Individual runs range from 2 to 10 h in duration, and the solute diffusion rates were determined in a different order for each membrane.

From the measured values of $S$, the slope of the $\ln \Delta C/\Delta C_0$ time plot, membrane area $A_m$, chamber volumes $V_1$ and $V_2$, an overall diffusion resistance $R_0$, was calculated for each run:

$$R_0 = \frac{A_m\left(\frac{1}{V_1} + \frac{1}{V_2}\right)}{S} \tag{14}$$

These values are displayed in Column 2 of Table VII.

In most instances, the diffusion rates given in Table VII represent the results from single runs. It should be noted, however, that each run is equivalent to a series of experiments in which diffusion is allowed to proceed for varying periods of time and solution concentrations then measured. When the membranes and diffusion system were kept scrupulously clean, these results were found to be quite reproducible. Of several duplicate runs, none differed by more than 2 %. The rate for urea in Membrane 48 was measured three separate times and values for $S$ of 12.93, 12.92, and $12.87 \cdot 10^{-5}$ $sec^{-1}$ were found. Similarly, $S$ values of 6.88 and $6.86 \cdot 10^{-5}$ $sec^{-1}$ were measured for glucose diffusion through Membrane 48.

TABLE VII

DIFFUSION RESULTS FOR MICA MEMBRANES

| *Solute* | $R_0$ (*sec/cm*) $\times 10^{-2}$ | $R_m$ (*sec/cm*) $\times 10^{-2}$ | *Pore radius from water flow data* | | | *Pore radius from extrapolation of diffusion data* | | |
|---|---|---|---|---|---|---|---|---|
| | | | $\mathscr{D}_m \times 10^6$ ($cm^2/sec$) | $\mathscr{D}_m/\mathscr{D}_0$ | $R_s/R_p$ | $\mathscr{D}_m \times 10^6$ ($cm^2/sec$) | $\mathscr{D}_m/\mathscr{D}_0$ | $R_s/R_p$ |
| | *Membrane 33* | | | $R_p = 306$ Å | | | $R_p = 292$ Å | |
| Urea | 22.3 | 14.2 | 12.2 | 0.886 | 0.0086 | 13.47 | 0.976 | 0.0090 |
| Glucose | 41.8 | 29.4 | 5.94 | 0.882 | 0.0145 | 6.54 | 0.972 | 0.0152 |
| Sucrose | 53.2 | 38.7 | 4.51 | 0.866 | 0.0181 | 4.97 | 0.954 | 0.0190 |
| Raffinose | 64.0 | 47.7 | 3.66 | 0.843 | 0.0213 | 4.03 | 0.929 | 0.0224 |
| α-Dextrin | 79.7 | 60.9 | 2.86 | 0.833 | 0.0261 | 3.15 | 0.917 | 0.0274 |
| β-Dextrin | 85.4 | 65.6 | 2.66 | 0.826 | 0.0277 | 2.93 | 0.910 | 0.0290 |
| | *Membrane 44* | | | $R_p = 119$ Å | | | $R_p = 110$ Å | |
| Urea | 30.7 | 22.6 | 10.59 | 0.767 | 0.0221 | 12.50 | 0.905 | 0.0240 |
| Glucose | 61.2 | 48.7 | 4.92 | 0.731 | 0.0372 | 5.81 | 0.863 | 0.0404 |
| Sucrose | 83.1 | 68.8 | 3.49 | 0.669 | 0.0464 | 4.11 | 0.790 | 0.0505 |
| Raffinose | 101.3 | 85.0 | 2.82 | 0.650 | 0.0547 | 3.33 | 0.768 | 0.0595 |
| α-Dextrin | 133.2 | 115.0 | 2.08 | 0.607 | 0.0669 | 2.46 | 0.716 | 0.0727 |
| β-Dextrin | 150 | 130.2 | 1.84 | 0.573 | 0.0710 | 2.17 | 0.676 | 0.0771 |
| Ribonuclease | 888 | 852 | 0.282 | 0.239 | 0.1808 | 0.33 | 0.282 | 0.1964 |
| | *Membrane 45* | | | $R_p = 172$ Å | | | $R_p = 166$ Å | |
| Urea | 13.6 | 5.58 | 12.06 | 0.874 | 0.0153 | 13.02 | 0.944 | 0.0159 |
| Glucose | 24.0 | 11.64 | 5.78 | 0.859 | 0.0257 | 6.24 | 0.928 | 0.0267 |
| Sucrose | 30.1 | 15.54 | 4.33 | 0.831 | 0.0322 | 4.67 | 0.897 | 0.0334 |
| Raffinose | 35.4 | 21.1 | 3.18 | 0.733 | 0.0379 | 3.43 | 0.792 | 0.0394 |
| α-Dextrin | 44.8 | 26.1 | 2.57 | 0.749 | 0.0464 | 2.78 | 0.809 | 0.0482 |
| β-Dextrin | 47.1 | 27.3 | 2.46 | 0.765 | 0.0492 | 2.66 | 0.827 | 0.0511 |
| Ribonuclease | 157.2 | 121.2 | 0.555 | 0.470 | 0.1252 | 0.600 | 0.508 | 0.1301 |
| | *Membrane 46* | | | $R_p = 169$ Å | | | $R_p = 170$ Å | |
| Urea | 13.56 | 5.52 | 13.25 | 0.960 | 0.0156 | 13.10 | 0.949 | 0.0155 |
| Glucose | 23.9 | 11.5 | 6.35 | 0.943 | 0.0262 | 6.27 | 0.932 | 0.0260 |
| Sucrose | 29.9 | 15.3 | 4.76 | 0.914 | 0.0327 | 4.70 | 0.903 | 0.0326 |
| Raffinose | 34.6 | 18.3 | 3.98 | 0.918 | 0.0386 | 3.93 | 0.907 | 0.0386 |
| α-Dextrin | 44.3 | 25.3 | 2.88 | 0.838 | 0.0472 | 2.85 | 0.829 | 0.0469 |
| β-Dextrin | 47.5 | 27.7 | 2.64 | 0.819 | 0.0500 | 2.60 | 0.810 | 0.0497 |
| Ribonuclease | 153.6 | 117.6 | 0.622 | 0.527 | 0.1274 | 0.615 | 0.5212 | 0.1267 |
| | *Membrane 47* | | | $R_p = 75$ Å | | | $R_p = 74.5$ Å | |
| Urea | 14.1 | 6.12 | 12.19 | 0.883 | 0.0352 | 12.35 | 0.895 | 0.0354 |
| Glucose | 26.0 | 13.6 | 5.47 | 0.814 | 0.0529 | 5.55 | 0.825 | 0.0596 |
| Sucrose | 34.6 | 20.0 | 3.72 | 0.714 | 0.0740 | 3.77 | 0.724 | 0.0745 |
| Raffinose | 42.4 | 26.1 | 2.85 | 0.658 | 0.0872 | 2.89 | 0.667 | 0.0878 |
| α-Dextrin | 53.9 | 35.1 | 2.12 | 0.617 | 0.1067 | 2.15 | 0.625 | 0.1074 |
| β-Dextrin | 57.7 | 37.8 | 1.97 | 0.613 | 0.1131 | 2.00 | 0.621 | 0.1138 |
| Ribonuclease | 378 | 342 | 0.218 | 0.184 | 0.2880 | 0.221 | 0.187 | 0.289 |

TABLE VII (continued)

| *Solute* | $R_0$ (*sec/cm*) $\times 10^{-2}$ | $R_m$ (*sec/cm*) $\times 10^{-2}$ | *Pore radius from water flow data* | | | *Pore radius from extrapolation of diffusion data* | | |
|---|---|---|---|---|---|---|---|---|
| | | | $\mathscr{D}_m \times 10^6$ (*cm²/sec*) | $\mathscr{D}_m/\mathscr{D}_0$ | $R_s/R_p$ | $\mathscr{D}_m \times 10^6$ (*cm²/sec*) | $\mathscr{D}_m/\mathscr{D}_0$ | $R_s/R_p$ |
| | *Membrane 48* | | | $R_p = 68.5$ Å | | | $R_p = 67.5$ Å | |
| Urea | 22.1 | 14.1 | 11.03 | 0.799 | 0.0385 | 11.36 | 0.823 | 0.0381 |
| Glucose | 31.5 | 29.1 | 5.33 | 0.793 | 0.0648 | 5.49 | 0.816 | 0.0658 |
| Sucrose | 55.4 | 40.8 | 3.80 | 0.731 | 0.0810 | 3.92 | 0.752 | 0.0822 |
| Raffinose | 68.4 | 52.0 | 2.98 | 0.688 | 0.0955 | 3.07 | 0.709 | 0.0969 |
| α-Dextrin | 93.7 | 75.0 | 2.07 | 0.603 | 0.1168 | 2.13 | 0.621 | 0.1185 |
| β-Dextrin | 105.2 | 85.4 | 1.82 | 0.565 | 0.1238 | 1.87 | 0.582 | 0.1256 |
| Ribonuclease | 1110 | 1074 | 0.144 | 0.122 | 0.3153 | 0.149 | 0.126 | 0.320 |
| | *Membrane 50* | | | $R_p = 58$ Å | | | $R_p = 58$ Å | |
| Urea | 17.28 | 9.24 | 12.17 | 0.882 | 0.0445 | 12.17 | 0.882 | 0.0445 |
| Glucose | 34.2 | 21.7 | 5.16 | 0.767 | 0.0766 | 5.16 | 0.767 | 0.0766 |
| Sucrose | 44.4 | 29.6 | 3.79 | 0.728 | 0.0957 | 3.79 | 0.728 | 0.0957 |
| Raffinose | 55.2 | 38.8 | 2.89 | 0.666 | 0.1128 | 2.89 | 0.666 | 0.1128 |
| α-Dextrin | 73.4 | 54.6 | 2.05 | 0.598 | 0.1379 | 2.05 | 0.598 | 0.1379 |
| β-Dextrin | 80.7 | 60.9 | 1.84 | 0.573 | 0.1462 | 1.84 | 0.573 | 0.1462 |
| Ribonuclease | 1050 | 1014 | 0.110 | 0.094 | 0.3724 | 0.110 | 0.094 | 0.3724 |
| | *Membrane 51* | | | $R_p = 45.7$ Å | | | $R_p = 44.4$ Å | |
| Urea | 21.7 | 15.7 | 10.87 | 0.788 | 0.0577 | 11.54 | 0.836 | 0.0595 |
| Glucose | 63.5 | 41.1 | 4.15 | 0.617 | 0.0970 | 4.41 | 0.655 | 0.1000 |
| Sucrose | 76.0 | 61.5 | 2.78 | 0.533 | 0.1213 | 2.95 | 0.566 | 0.1250 |
| Raffinose | 99.6 | 80.8 | 2.11 | 0.487 | 0.1430 | 2.24 | 0.517 | 0.1473 |
| α-Dextrin | 148.2 | 129.6 | 1.313 | 0.383 | 0.1749 | 1.40 | 0.407 | 0.1802 |
| β-Dextrin | 168.6 | 148.8 | 1.149 | 0.356 | 0.1854 | 1.22 | 0.378 | 0.1910 |

The membrane resistances for each solute reported in Column 3 of Table VII were then obtained by subtracting from each $R_0$, the corresponding values for the boundary layer resistance given in Table VI for the same solute. Note that implicit in this procedure is the assumption that both the membrane permeability and boundary layer resistances are uniform over the entire surface of the membrane. As pointed out earlier, the boundary layer was not uniform in our diffusion cell, however, the effect of the variation in boundary layer resistance was less than 0.7 % in these studies (see APPENDIX).

*Hindered diffusion within membrane pores*

To calculate the apparent mean diffusion coefficients of the solutes in the mica membranes requires an estimate of the total cross-sectional area of the pores (the open area is uniform throughout the thickness of the membrane), and the pore length. The corrected pore lengths are obtained from thickness measurements as described earlier. The open cross-sectional area of the membrane can be estimated in three ways: from

the water flow measurements, from the air flow measurements, and from the diffusion measurements. These methods yield slightly different results for the magnitude of hindered diffusion within the membrane, but at the same time provide independent confirmation for the results.

The apparent diffusivity of a molecule within the pores of the membranes is obtained from the estimated values of the membrane resistance

$$\mathscr{D}_m = \frac{L}{R_m n_0 A_p} \tag{15}$$

The cross-sectional pore area per unit surface area of the membrane, $A_p$, was found from water flow, air flow, and diffusion data. There was some discrepancy between estimates of pore area based on air flow and water flow data. As mentioned earlier, there is reason to have more confidence in pore size as measured by the water flow than air flow and, in addition, the fact that the diffusion studies were conducted in an entirely aqueous medium is another reason for giving more weight to the water flow method.

The apparent diffusion coefficient of the solutes within the pores of the membrane, $\mathscr{D}_m$, given in Column 4 of Table VII is based on water flow measurements. The ratio of the solute diffusion coefficient within the membrane and the free diffusion coefficient of the same solute, $\mathscr{D}_0$, is given in the next column of Table VII.

In all cases the diffusion coefficient of a solute within a pore is less than its value in free solution. This is clear evidence that there is a hindrance of diffusion inside microporous materials. Also, these data are negative evidence for supposing that surface diffusion plays an important role for the solutes and membrane material used in this study. If adsorption of solute to the pore walls and subsequent diffusions of solute contributed significantly to the net flux of solute through the pores, then the overall apparent diffusion coefficient of solutes within the membranes would be expected to be greater than its diffusivity in free solution.

To correlate the extent of diffusion hindrance with pore size, the pore radius corresponding to a circle of area equal to the oval was used, Eqn. 3b. The pore radius as determined by this method is given for each membrane at the head of Columns 4, 5, and 6.

This set of hindered diffusion data is plotted in Fig. 11. A rather substantial reduction in diffusion coefficients occurs even at low ratios of solute radius to pore size.

Another procedure for estimating pore size independent of the flow method also leads to similar results for the magnitude of diffusion hindrance by pores. If the diffusion rate of a solute, small enough so that it was not subject to hindrance by the pores, is measured, then the cross-sectional pore area can be calculated directly. This is essentially the principle behind Pappenheimer's method for estimating pore area by the measurement of the diffusion rate of labelled water through a membrane. The diffusion of labelled water was not measured in these studies, but the diffusion data for the other solutes can be extrapolated to give similar information.

As seen in Fig. 11, the ratio $\mathscr{D}_m/\mathscr{D}_0$ is a function of the ratio of molecular size to pore size; say $f(R_s/R_p)$, where $f(R_s/R_p)$ approaches 1 as $R_s/R_p \to 0$. Now for any solute, if $R_m$ is the membrane diffusion resistance, then from Eqn. 15:

$$\mathscr{D}_m = \frac{L}{R_m n_0 A_p}$$

and substituting for $\mathscr{D}_m = \mathscr{D}_0 \cdot f(R_s/R_p)$ and $A_p = \pi R_p^2$

$$f\left(\frac{R_s}{R_p}\right) R_p^2 = \frac{L}{\pi R_m n_0 \mathscr{D}_0} \tag{16}$$

All the quantities on the right hand side are either known or measured, so that within a series of solutes for each membrane, the group $(L/\pi R_m n_0 \mathscr{D}_0)$ can be calculated for each solute. If the group $(L/\pi R_m n_0 \mathscr{D}_0)$ is plotted against $R_s$, a curve is obtained and recalling that as $R_s \to 0$, $f(R_s/R_p) \to 1$ the intercept of this curve extrapolated to $R_s \to 0$ gives $R_p^2$.

Sample extrapolations of this nature are given in Fig. 12. The curves are fairly linear in the region of measurements which gives some confidence in the extrapolation procedure. Using these estimates for the pore diameter, effective solute diffusion coefficients within the pores can be calculated as before. The results for this extrapolation procedure are given in the last three columns of Table VII. When these values are plotted as before, a similar pattern is obtained as shown in Fig. 13. The relative scatter of the data in the latter figure is less than the former, but this seemingly more consistent result is only a reflection of the fact that in the extrapolation procedure, the lines were essentially force fit to go through the same point, *i.e.* $\mathscr{D}_m/\mathscr{D}_0 = 1$, $R_s/R_p = 0$.

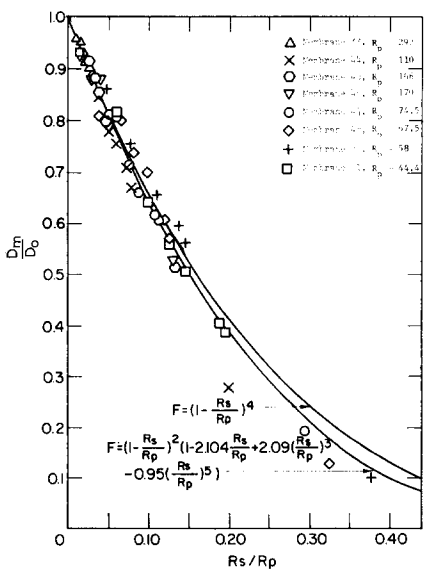


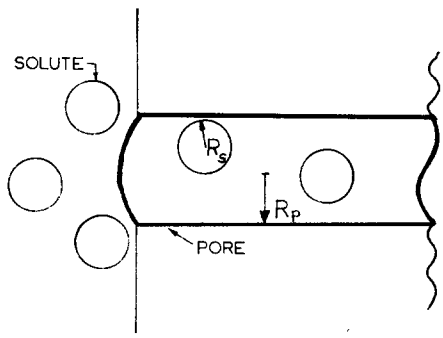


Fig. 13. Ratio of solute diffusivity in membrane pore to solute diffusivity in free solution, $\mathscr{D}_m/\mathscr{D}_0$, as a function of the ratio of solute radius to pore radius, $R_s/R_p$. Pore radius determined from extrapolation of diffusion data.

Fig. 14. Cylindrical model of a membrane pore. Ratio of solute concentration within the pore to solute concentration in free solution is $(1-R_s/R_p)^2$.

## DISCUSSION

The experimental results obtained here clearly demonstrate that the mobility of molecules through molecular-size pores is significantly less than their mobility through the same cross-sectional area of free solution. Also, the decrease in mobility is directly correlated with the relative ratio of molecular size to pore size. Reasons for this behavior are not at all obvious.

The explanation for hindered diffusion that has developed over the years is related to two different phenomenological concepts. One idea, first proposed by FERRY[37], is that molecules are excluded from small pores because of statistical effects related to the relative size of molecules and pores. Although Ferry pictured the effect as due to the reflection of molecules away from a pore opening if the trajectory of a molecule is within one molecular radius of the pore wall, present day concepts see the effect as an exclusion phenomena based on limited space for molecules within small pores (ACKERS[38]). In fact, the exclusion effect is one of the basic ideas which is used to explain separations by gel permeation chromatography[39–41]. As applied to a simple circular pore, the exclusion effect simply states that at equilibrium a concentration distribution will develop between the pore and outside solution given by the geometric factors as shown in Fig. 14.

$$f_e = \frac{c_p}{c_s} = \left[1 - \left(\frac{R_s}{R_p}\right)^2\right]$$

where $c_s$ is the solute concentration in free solution at the membrane interface, and $c_p$ is the solute concentration within the pore. If the pores had a different geometry, as a series of cones, spheres, or random spaces between rods, the exclusion factors or concentration ratios would be different[39,42,43].

The geometric exclusion hypothesis neglects the possibility of surface adsorption within the pore or the opposite effect of repulsion of solute near an interface[44]. The magnitude of such surface–solute interactions would of course depend on the specific chemical and electrical properties of the surface and solutes, as suggested by the Gibbs surface isotherm.

The exclusion hypothesis only pertains to the equilibrium distribution of solute. But in applying this effect to diffusion within pores, a further assumption is made that the diffusion flux is proportional to the gradient in solute concentration within the pores. This effect alone would result in a reduction of solute diffusion rate, $N_s$, through a membrane as compared to free solution by an amount equal to the exclusion ratio, *i.e.*,

$$N_s \propto \Delta c_p \propto f_e \Delta c_s$$

where $\Delta c_p$ and $\Delta c_s$ are differences in solute concentrations across the pores and membrane surface directly.

However, the magnitude of postulated effects were not sufficient to explain reduced diffusion rates through membranes and LANE[45] suggested that hindrance was due to an increase in drag on the solute molecule as it traversed a pore, analogous to the increase in drag on a sphere falling in a capillary tube of comparable diameter. The drag effect results in decrease in the diffusivity by the factor $f_d$:

$$f_d = 1 - 2.104\left(\frac{R_s}{R_p}\right) + 2.09\left(\frac{R_s}{R_p}\right)^3 - 0.95\left(\frac{R_s}{R_p}\right)^5 \tag{17}$$

If drag alone were the causitive factor for lower fluxes through membranes then the flux would be reduced by $f_d$. However, neither of these alone accounts for the experimental data, and PAPPENHEIMER[5] and RENKIN[6] suggested that the product of these effects may account for the experimental results.

$$N_s = f_e f_d \mathscr{D}_0 A_p n_0 \Delta c_s \tag{18}$$

The product $f_e f_d \mathscr{D}_0 = \mathscr{D}_m$ gives an estimate of the effective diffusion coefficient $\mathscr{D}_m$ of solutes within a microporous membrane, or

$$\frac{\mathscr{D}_m}{\mathscr{D}_0} = f_e f_d = \left[1 - \left(\frac{R_s}{R_p}\right)^2\right]\left[1 - 2.104\left(\frac{R_s}{R_p}\right) + 2.09\left(\frac{R_s}{R_p}\right)^3 - 0.95\left(\frac{R_s}{R_p}\right)^5\right] \tag{19}$$

This expression, first given by RENKIN[6], is plotted in Fig. 11 and Fig. 13 and shows excellent agreement with our experimental data. However, the degree of correlation may be fortuitous in that the concepts concerning the separate factors $f_e$ and $f_d$ may not be correct individually, but the product of these factors may be self-compensating for systematic errors.

We believe that the numerical prediction given by Eqn. 19 may be used to estimate hindrance effects on spherical molecules within cylindrical pores, especially in the range of $R_s/R_p$ less than 0.2, but the concepts used in obtaining this equation need further verification.

An interesting application of the results obtained here is to estimate the effect of wider pore size distributions on separation of solutes by dialysis. Photomicrographs of dialysis membranes[46] usually show the membrane to be much more heterogeneous in pore size and shape than the membranes in this work. Structural heterogeneity may display its influence in two ways; (1) in a wide distribution of pore sizes and (2) in a wide distribution of tortuosities, *i.e.* increasing tortuosity with larger molecular size[47].

Estimates of these effects can be made using Eqn. 19 and on some reasonable guesses for the distribution functions for pore size and pore length. Let us assume that pore cell lengths in a conventional dialysis membrane are the same but the pore size is normally distributed with a mean radius $\bar{R}_p$ and standard deviation $\sigma$. The diffusion flux of a solute molecule of radius $R_s$ per unit membrane area is given by:

$$N_s = \mathscr{D}_0 n_0 \int_{\substack{\bar{R}_p - 3\sigma \\ \text{or } Rs}}^{\bar{R}_p + 3\sigma} \frac{f_e f_p R_p^2 e^{-(R_p - \bar{R}_p)^2/2\sigma^2} \sqrt{\pi} \mathrm{d}P_p}{\sqrt{2}\sigma} \tag{20}$$

where the limits $\pm$ 3 $\sigma$ account for 99,9 % of the pores, and the lower limit is $R_s$ or $\bar{R}_p$ —3 $\sigma$, whichever is larger. The effective diffusivity ratio $\mathscr{D}_m/\mathscr{D}_0$ of a molecule in a heteroporous membrane is given by:

$$\frac{\overline{\mathscr{D}}_m}{\mathscr{D}_0} = \frac{\int f_e f_p R_p^2 e^{-(R_p-\bar{R}_p)^2/2\sigma^2} dR_p}{\int R_p e^{-(R_p-\bar{R}_p)^2/2\sigma^2} dR_p} \tag{21}$$

where the limits on the integrals are the same as given in Eqn. 20. Parametric curves of this function for different variances of the pore size distribution is given in Fig. 15.

The results are somewhat surprising in that for molecules less than 20% of the mean pore size, pore size distribution has a little effect. In other words, isoporous membranes are of little advantage in separating solutes by diffusion if the sizes of the molecules being separated are less than 20 % of the mean pore size.

In the region of higher ratios of solute to pore size, there seems to be a definite advantage to isoporous membranes for separation effectiveness. However, it must be remembered that Eqn. 19 has not been experimentally verified in this region and therefore predictions from Fig. 15 must be used with caution when $R_s/\bar{R}_p > 0.2$. If the tortuosity increases with molecular size, then this type of heterogeneous membrane

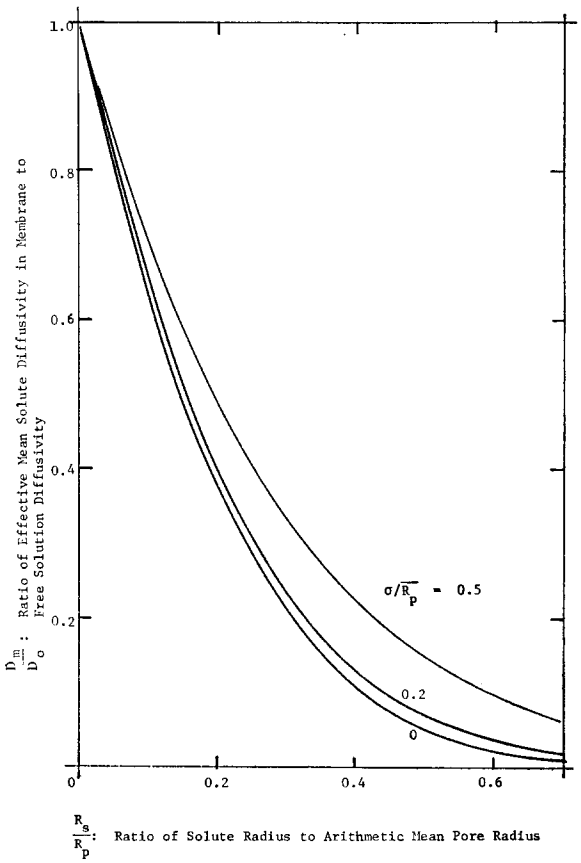


Fig. 15. Assuming pore sizes in membranes are normally distributed, this graph shows the effect of the variance of pore size distribution on the apparent mean diffusivities, $\overline{\mathscr{D}}_m$, of solutes in the membranes. Hindrance factors, $\overline{\mathscr{D}}_m/\mathscr{D}_0$, were calculated from the Renkin equation, Eqn. 19. The curves are drawn for different values of the parameter $\sigma/\bar{R}_p$, the ratio of the standard deviation of the pore size distribution to the arithmetic average mean pore radius.

will be more selective that the heteroporous-isolength membranes represented in Fig. 15. No data are presently available on the distribution of tortuosity with solute size for real membranes, and calculations of this effect will need to await future experimental work.

Some estimates of the heteroporosity of membranes can be made from diffusion experiments and an estimate of the mean pore size. The curves in Fig. 15 can be linearized appreciably if $\bar{\mathscr{D}}_m/\mathscr{D}_0$ is plotted against $(1-R_s/\bar{R}_p)$ on log–log paper, as shown in Fig. 16.

The curves can be approximated by straight lines in the region of $1 < R_s/\bar{R}_p < 0.5$, *i.e.* in this region the curves can be approximated by the equation:

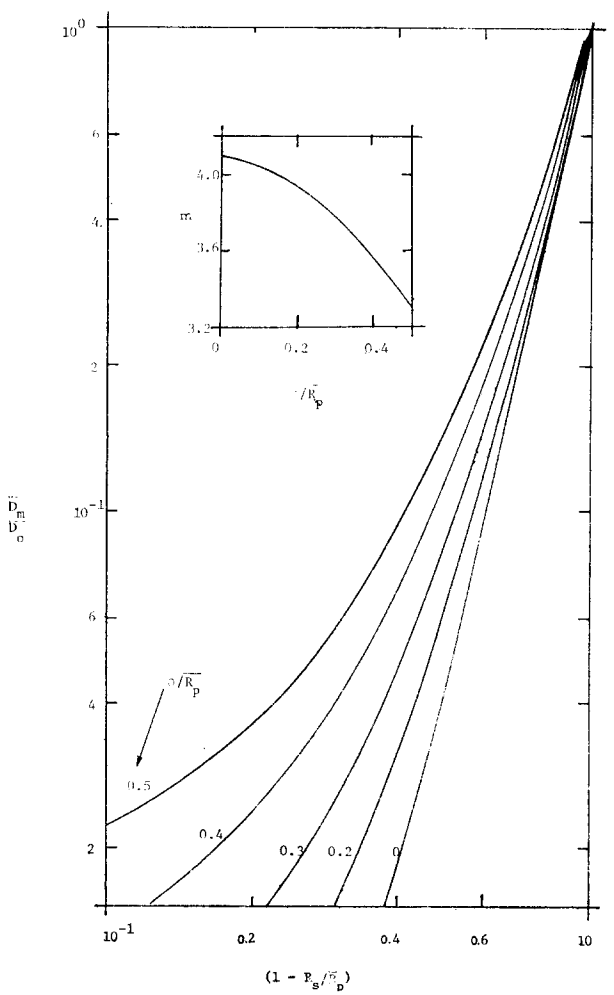


Fig. 16. Diagnostic curves for estimating pore size distributions in membranes. Plots of log $(\bar{\mathscr{D}}_m/D_0)$ *vs.* log $(1-R_s/R_p)$ result in nearly straight lines in the region of $(1-R_s/R_p) > 0.5$. The slope of the parametric curves for $(1-R_s/R_p) > 0.5$ *vs.* the normalized pore size standard deviation, $\sigma/\bar{R}_p$, is given in the insert.

$$\frac{\bar{\mathscr{D}}_m}{\mathscr{D}_0} \approx \left(1 - \frac{R_s}{\bar{R}_p}\right)^m \tag{19a}$$

For this region the slope of the curve, $m$, is directly related to the standard deviation ($\sigma$) of the pore size distribution as shown in the inset. For an isoporous membrane, the slope $m$ is approx. 4, indicating that Eqn. 19a with $m = 4$ may be a satisfactory approximation to the more complicated Renkin equation, Eqn. 19.

Thus, some information on the pore size distribution of a membrane can be obtained by plotting the membrane permeabilities for a graded series of solutes and plotting the permeabilities against $(1-R_s/\bar{R}_p)$ on log-log paper. The slope in the region $(1-R_s/\bar{R}_p) > 0.5$ is obtained and from the inset in Figure 16, an estimate of $\sigma$ is obtained. In order to use this technique, one needs to know $\bar{R}_p$, which can be obtained by methods mentioned previously. Also, in using this method one must correct for boundary layer effects in determining the membrane permeability.

## APPENDIX

A source of systematic error in the film resistance results is the nonuniformity of the flow conditions within the diffusion chambers. One problem here is that the mean film resistances for the four squares that make up the total membrane area are not the same. This means that the film resistances for the Nuclepore, Millipore, and mica membranes are not strictly comparable.

To illustrate this and to estimate its effect, assume that the transfer area consists of 4 squares of equal area with film resistances $R_{f_1}$, $R_{f_2}$, $R_{f_3}$, and $R_{f_4}$, respectively. Then the mean film resistance in the absence of a membrane resistance (corresponding to the electrochemical experiments) is:

$$\frac{1}{R_{fm}} = \frac{1}{4}\left(\frac{1}{R_{f1}} + \frac{1}{R_{f2}} + \frac{1}{R_{f3}} + \frac{1}{R_{f4}}\right) \tag{22}$$

However, when the film resistance is in series with a membrane resistance, a somewhat different mean will be measured. This apparent resistance, $R'_{fm}$, is given by the equation:

$$\frac{1}{R_m + 2R'_{fm}} = \frac{1}{4}\left[\frac{1}{R_m + 2R_{f1}} + \frac{1}{R_m + 2R_{f2}} + \frac{1}{R_m + 2R_{f3}} + \frac{1}{R_m + 2R_{f4}}\right] \tag{23}$$

The individual resistances can be calculated from the electrochemical results as: $R_{f_1} = 1.16\ R_{fm}$, $R_{f_2} = 1.32\ R_{fm}$, and $R_{f_3} = R_{f_4} = 0.85\ R_{fm}$. Therefore Eqn. 24 is obtained:

$$\frac{1}{R_m + 2R'_{fm}} = \frac{1}{4}\left[\frac{1}{R_m + 1.16 \cdot 2R_{fm}} + \frac{1}{R_m + 1.32 \cdot 2R_{fm}} + \frac{1}{R_m + 0.84 \cdot 2R_{fm}}\right] \tag{24}$$

Eqn. 19 can be rearranged to give the percentage difference between the apparent resistance in the presence of a membrane resistance and that in its absence:

$$100\frac{R'_{fm} - R_{fm}}{R_{fm}} = \frac{16.1\varepsilon^2 + 19.4\varepsilon}{4\varepsilon^2 + 9.12\varepsilon + 5.15} \tag{25}$$

where

$$\varepsilon = R_m/R_{fm}$$

Using Eqn. 20 to calculate the film resistances which are applicable to each of the mica membranes shows that the nonuniformity in flow conditions caused an error of less than + 0.7 % in the calculated mica membrane resistances.

ACKNOWLEDGEMENTS

This work was supported in part by Public Health Service Grant GM 15152, and by a Research Career Development Award (Number 1-K4-GM-8271) to Jerome S. Schultz from the Institute of General Medical Sciences. Shyam Suchdeo assisted in the numerical calculations.

REFERENCES

1 R. COLLANDER, *Kolloid-Behefte*, 19 (1924) 72.
2 L. MICHAELIS, *Kolloid Z.*, 62 (1933) 2.
3 E. MANGOLD, *Kolloid Z.*, 49 (1929) 372.
4 H. SPANDAU AND W. GROSS, *Chem. Ber.*, 74B (1941) 362.
5 J. R. PAPPENHEIMER, *Physiol. Rev.*, 33 (1953) 387.
6 E. M. RENKIN, *J. Gen. Physiol.*, 38 (1954) 225.
7 E. FUCHS AND G. GORIN, *Biochem. Biophys. Res. Commun.*, 5 (1961) 196.
8 B. M. UZELAC AND E. L. CUSSLER, *J. Colloid Sci.*, 32 (1970) 487.
9 R. L. FLEISCHER AND P. B. PRICE, *Science*, 140 (1963) 1221.
10 R. L. FLEISCHER, P. B. PRICE AND R. M. WALKER, *Rev. Sci. Instrum.*, 34 (1963) 510.
11 R. L. FLEISCHER, P. B. PRICE AND E. M. SYMES, *Science*, 143 (1964) 249.
12 R. L. FLEISCHER, P. B. PRICE AND R. M. WALKER, *J. Appl. Phys.*, 36 (1965) 3645.
13 R. L. FLEISCHER, P. B. PRICE AND R. M. WALKER, *Science*, 149 (1965) 383.
14 P. B. PRICE AND R. M. WALKER, *J. Appl. Phys.*, 33 (1962) 3400.
15 P. B. PRICE AND R. M. WALKER, *J. Appl. Phys.*, 33 (1962) 3407.
16 P. B. PRICE AND R. M. WALKER, *Phys. Lett.*, 3 (1962) 113.
17 C. P. BEAN, U.S. Department of Interior, Research and Development Progress Report No. 465, 1969.
18 C. P. BEAN, M. V. DOYLE AND G. ENTINE, *J. Appl. Phys.*, 41 (1970) 1454.
19 R. E. BECK AND J. S. SCHULTZ, *Science*, 170 (1970) 1302.
20 K. V. MARSH AND J. A. MISKEL, *J. Inorg. Nucl. Chem.*, 21 (1961) 15.
21 R. E. BECK, Ph.D. Dissertation, University Microfilms, Ann Arbor, Mich., 1969.
22 W. HALLER, *Nature*, 206 (1965) 693.
23 D. I. HITCHCOCK, *J. Gen. Physiol.*, 9 (1926) 755.
24 O. KEDEM AND A. KATCHALSKY, *J. Gen. Physiol.*, 45 (1961) 143.
25 V. KOEFFED-JOHNSON AND H. USSIG, *Acta Physiol. Scand.*, 28 (1953) 60.
26 N. LAKSHMINARAYANAIAH, *Biophys. J.*, 7 (1967) 511.
27 H. FOK, V. GOLDANSKII AND N. CHIRKOV, *Dokl. Akad. Nauk SSSR*, 61 (1948) 673.
28 D. FRENCH, *Adv. Carbohydr. Chem.*, 12 (1957) 190.
29 A. GIERER AND K. WIRTZ, *Z. Naturforsch.*, 8a (1953) 532.
30 W. H. ORTTUNG, *J. Phys. Chem.*, 67 (1963) 503.
31 V. LEVICH, *Physicochemical Hydrodynamics*, Prentice-Hall, Englewood Cliffs, N.J., 1962.
32 I. M. KOLTHOFF AND J. J. LINGANE, *Polarography*, Interscience, New York, 1941.
33 R. B. BIRD, W. E. STEWART AND E. N. LIGHTFOOT, *Transport Phenomena*, J. Wiley, New York, 1960.

34 D. JAHN AND W. VIELSTICH, *J. Electrochem. Soc.*, 109 (1962) 849.
35 K. A. SMITH, C. K. COLTON, E. W. MERRILL AND L. B. EVANS, *Chem. Eng. Prog. Symp. Ser. No. 84*, 64 (1968) 45.
36 A. L. BABB, C. MAURER, D. FRY, R. POPOVICH AND R. MCKEE, *Chem. Eng. Prog. Symp. Ser. No. 84*, 64 (1968) 59.
37 J. D. FERRY, *Chem. Rev.*, 18 (1936) 373.
38 G. K. ACKERS, *Adv. Prot. Chem.*, 24 (1970) 343.
39 J. PORATH AND P. FLODIN, *Nature*, 183 (1959) 1657.
40 P. G. SQUIRE, *Arch. Biochem. Biophys.*, 107 (1964) 471.
41 T. C. LAURENT AND J. KILLANDER, *J. Chromatogr.*, 14 (1964) 317.
42 G. K. ACKERS, *J. Biol. Chem.*, 242 (1967) 3237.
43 A. G. OGSTON, *Trans. Faraday Soc.*, 54 (1958) 1754.
44 S. SOURIRAGAN, *Ind. Eng. Chem. (Fund.)*, 2 (1962) 51.
45 J. A. LANE, in J. H. PERRY, *Chemical Engineer's Handbook*, McGraw-Hill, New York, 1950, p. 753.
46 J. C. BUGHER, *J. Gen. Physiol.*, 36 (1953) 431.
47 J. S. SCHULTZ AND P. GERHARDT, *Bact. Rev.*, 33 (1969) 1.
48 L. G. LONGSWORTH, *J. Am. Chem. Soc.*, 75 (1953) 5705.
49 L. C. CRAIG, *Science*, 144 (1964) 1093.
50 F. J. JOUBERT AND T. HAYLETT, *J. S. Afr. Chem. Inst.*, 15 (1962) 48.
51 B. Z. GINZBURG AND A. KATCHALSKY, *J. Gen. Physiol.*, 47 (1963) 403.